LHCB 98-045 TRAC
February 18, 1998

Track Reconstruction For LHCB

Rutger van der Eijk [a], *Gonzalo Gracia* [a], *Marcel Merk* [b,1],
Werner Ruckstuhl [a], *Olaf Steinkamp* [a]

[a] NIKHEF Amsterdam [b] University of Utrecht

Abstract

In this note we describe the track reconstruction for LHCB. We apply a Kalman filter technique both for trackfitting and for trackfinding tasks. We demonstrate that the fit gives track parameters with correct errors. We then use the track reconstruction to find optimal positions for the location of tracking stations in the detector. For the final chosen setup we discuss performance numbers on track momentum and vertex position measurements, and for the invariant mass resolution of the D_s and B^0 mesons.

1 Introduction

The aim of the study described in this note was the overall optimization of the tracking system for LHCB. The following two questions were addressed:

- What is the optimum number of tracking stations and where should they be positioned?
- What performance can be obtained in terms of momentum, vertex and mass resolution?

A dedicated study dealing with the layout and segmentation of tracking stations is described in a separate note [1].

For the study presented here, a track reconstruction algorithm based on a Kalman-Filter technique has been implemented in the LHCB Monte-Carlo simulation package SICB [2]. Chapter 2 of this note is dedicated to a description of this tracking algorithm. In chapter 3, we describe the proposed detector configuration, and in chapter 4 we demonstrate the performance of this tracking system in terms of reconstruction of momenta and impact parameters.

[1] The research of M. Merk has been made possible by a fellowship of the Royal Netherlands Academy of Arts and Sciences.

2 Track Fitting With A Kalman-Filter Method

The Kalman-Filter algorithm used in this study is based on a code developed by the HERA-B collaboration. A detailed description of the method and its mathematical background can be found in a HERA-B note [3]. We restrict our discussion of Kalman Filters to a brief introduction in section 2.1 of this chapter. The particularitites of implementation for the different detector technologies and geometries employed in the LHCB tracking system are summarized in section 2.2. The parametrization of the multiple scattering and energy loss suffered by charged particles traversing the detector material are described in section 2.3. In section 2.4 we demonstrate the correct performance of the program.

2.1 The Kalman-Filter Technique

The aim of the track fit is the reconstruction of the full track state vector and the corresponding covariance matrix, from measured track impact points in a sequence of detection planes vertical to the beam axis (z axis). We have chosen to parametrize the track state vector as (x, y, t_x, t_y, κ), where the slopes are defined as $t_x = p_x \,/\, p_z$ and $t_y = p_y \,/\, p_z$ and the "curvature" as $\kappa = Q \,/\, p_\perp$, where $p_\perp$ is the component of the momentum perpendicular to the magnetic field, and Q the charge of the track.

The Kalman Filter technique is a recursive method, following a track candidate step by step through the detection planes. At each step, a new measurement is added to the track and the state vector and covariance matrix are updated. The improved knowledge of the track is used to define a search window in the following detection plane.

In the final result, the Kalman Filter method is mathematically equivalent to a global least-squares fit. However, it combines several advantages which make it very attractive for track reconstruction in LHCB:

- the tasks of track finding (pattern recognition) and track fitting are efficiently combined in one algorithm;
- the progressive inclusion of measurements avoids the need for a time-consuming global fit;
- perturbations of tracks due to multiple scattering and energy loss in the detector material can be included very efficiently, also for inhomogenuous distributions of material;
- it is straightforward to include different detection technologies in the track fit (e.g. inner tracker, outer tracker, vertex detector, etc.).

Particularly attractive for experiments as HERA-B and LHCB is so-called upstream tracking, starting the track search in the most downstream detection plane, behind the magnet, and following the track "backwards" towards the production vertex. This has the advantage that already the first measurements, together with an approximate knowledge of the production vertex, allow at a very early stage a rather precise prediction of the track momentum. A good estimate of the track momentum is crucial to keep search windows small when extrapolating the track into the magnetic field. Downstream tracking, on the contrary, seriously suffers from the lack of knowledge of track momentum. On entering the magnetic field, the momentum is still unknown, therefore the size of search window increases drastically, leading easily to unacceptably high numbers of "wrong" (combinatorial) track candidates.

2.2 Detector Technologies

The Kalman method allows to merge hit information from different detector technologies and geometries in the fit. For our study, the following detectors have been included:

- outer tracker, honeycomb drift chambers with wires running vertically and under two stereo angles
- inner tracker, planar detectors (MSGC, MCSC, Silicon) measuring the same angles as the outer tracker.
- vertex detector, silicon strips in "r / ϕ" geometry, where "ϕ" strips are slightly tilted

In all detection planes a one-dimensional measurement of the track position is made. This measured quantity is projected onto the track state vector and used in the fit:

1. in the outer tracker, a measurement of the closest distance of approach Δu of a track to a detection wire is done; in general, the wire is tilted by a stereo angle α_{st} with respect to the vertical;
2. all proposed options for the inner tracker are strip detectors, a direct measurement of one track coordinate is made; the detection strip is tilted by a stereo angle α_{st} with respect to the vertical;
3. vertex silicon r strips measure directly the radius of the impact point with respect to the beam axis (z axis);
4. vertex silicon ϕ strips are treated equivalent to inner tracker strips measuring a stereo angle $\alpha_{st} = \phi$.

detector:	(1)	(2)	(3)	(4)
$\frac{\partial h}{\partial x}$	$\cos\alpha_{st}\ \frac{1}{\sqrt{1+t_u^2}}$	$\cos\alpha_{st}$	$\frac{x}{\sqrt{x^2+y^2}}$	$\cos\alpha_{st}$
$\frac{\partial h}{\partial y}$	$\sin\alpha_{st}\ \frac{1}{\sqrt{1+t_u^2}}$	$\sin\alpha_{st}$	$\frac{y}{\sqrt{x^2+y^2}}$	$\sin\alpha_{st}$
$\frac{\partial h}{\partial t_x}$	$-\Delta u\frac{t_u}{\sqrt{1+t_u^2}^3}\cos\alpha_{st}$	0	0	0
$\frac{\partial h}{\partial t_y}$	$-\Delta u\frac{t_u}{\sqrt{1+t_u^2}^3}\sin\alpha_{st}$	0	0	0
$\frac{\partial h}{\partial \kappa}$	0	0	0	0

Table 1: Projection matrix elements ($\partial h/\partial q_i$) for track-parameter measurements from (1) outer tracker, (2) inner tracker, (3) silicon r strips and (4) silicon ϕ strips, with $t_u = t_x\cos\alpha_{st}+t_y\sin\alpha_{st}$, and $\Delta u = x\cos\alpha_{st}+y\sin\alpha_{st}-u_{wire}$.

The relation between the measured quantity and the track parameters (q_i) is called the projection matrix (h). Since the projection matrix elements depend on the detector geometries and are specific to the LHCB implementation, we list them explicitly in table 1.

2.3 Multiple Scattering and Energy Loss

After passing through a thin layer of material of thickness t (expressed in radiation lengths X_0) a minimum ionising particle undergoes a change of direction (multiple scattering), for which the variance is [4]:

$$(\,\delta\theta\,)^2 = \left(\frac{0.0136}{p}\right)^2 \cdot t \cdot (\,1+0.038\ \ln\,t\,)^2 \cdot f_{ms}^2$$

This additional variance is taken into account by enlargening the entries in the covariance matrix for the slope and momentum related parameters t_x, t_y and κ accordingly [3]. The correction factor f_{ms} is introduced to compensate for the non-Gaussian tail of multiple scattering events. It has been tuned such that the *average* scattering angle is taken into account correctly. We find a value of $f_{ms} = 1.3$.

The energy loss of a track passing through a layer of material of thickness t (in X_0) is strongly dependent on the particle type.

Any charged particle loses energy by ionisation, according to the Bethe-Bloch formula. Although these energy losses are small, they cannot be completely neglected for a momentum measurement on the per mille level. In principle, the energy loss of a minimum ionizing particle depends slightly on

the nuclear properties of the material it traverses. We do, however, assume a universal value of:

$$\left(\frac{dE}{dx}\right)_{coll} = 50\mathrm{MeV/X_0}$$

for all materials. The value of 50 MeV has been tuned to obtain for the reconstructed momenta the same average as for the generated momenta. The average amount of material seen by a minumum ionising particle up to the RICH2 is about 20% of a radiation length, corresponding to an integrated energy loss of about 10 MeV.

For electrons the energy loss is dominated by emission of radiation ("Bremsstrahlung") and is of the form [6]:

$$\left(\frac{dE}{dx}\right)_{rad} = \frac{E}{X_0}$$

with X_0 the radiation length of the material. The ratio of energies of the incoming and outgoing track is thus:

$$\left\langle \frac{E_{out}}{E_{in}} \right\rangle = e^{-t}$$

This leads to a contribution to the variance of the momentum measurement of [5, 3]:

$$(\delta\kappa)^2 = \kappa^2 \ \left(e^{-t\frac{\ln 3}{\ln 2}} - e^{-2t}\right)$$

2.4 Program Performance

A measure for the reliability of the fit are the *pull* distributions, namely difference of reconstructed and generated quantity, divided by the error given by the fit. We show these pull distributions for all track parameters, at the z position of the generated track origin, in figure 1. The reconstructed track parameters and covariance matrices have been extrapolated from the first measurement to this z position, taking into account all materials. The plots show that for all five trackparameters the average of the reconstructed value is equal to the generated value. In addition, the distributions have a width of one, demonstrating that the reconstructed error correctly describes the difference between reconstructed and generated values.

In figure 2 we show the chisquared probability distribution for the trackfit. The plot shows a horizontal distribution, except for a few lower and upper bins. The peak at zero probabilities is due to the non-Gaussian tail in the multiple scattering distribution. Only for Gaussianly distributed scattering angles a correct χ^2 is expected, a non-Gaussian tail yields an acecess of events

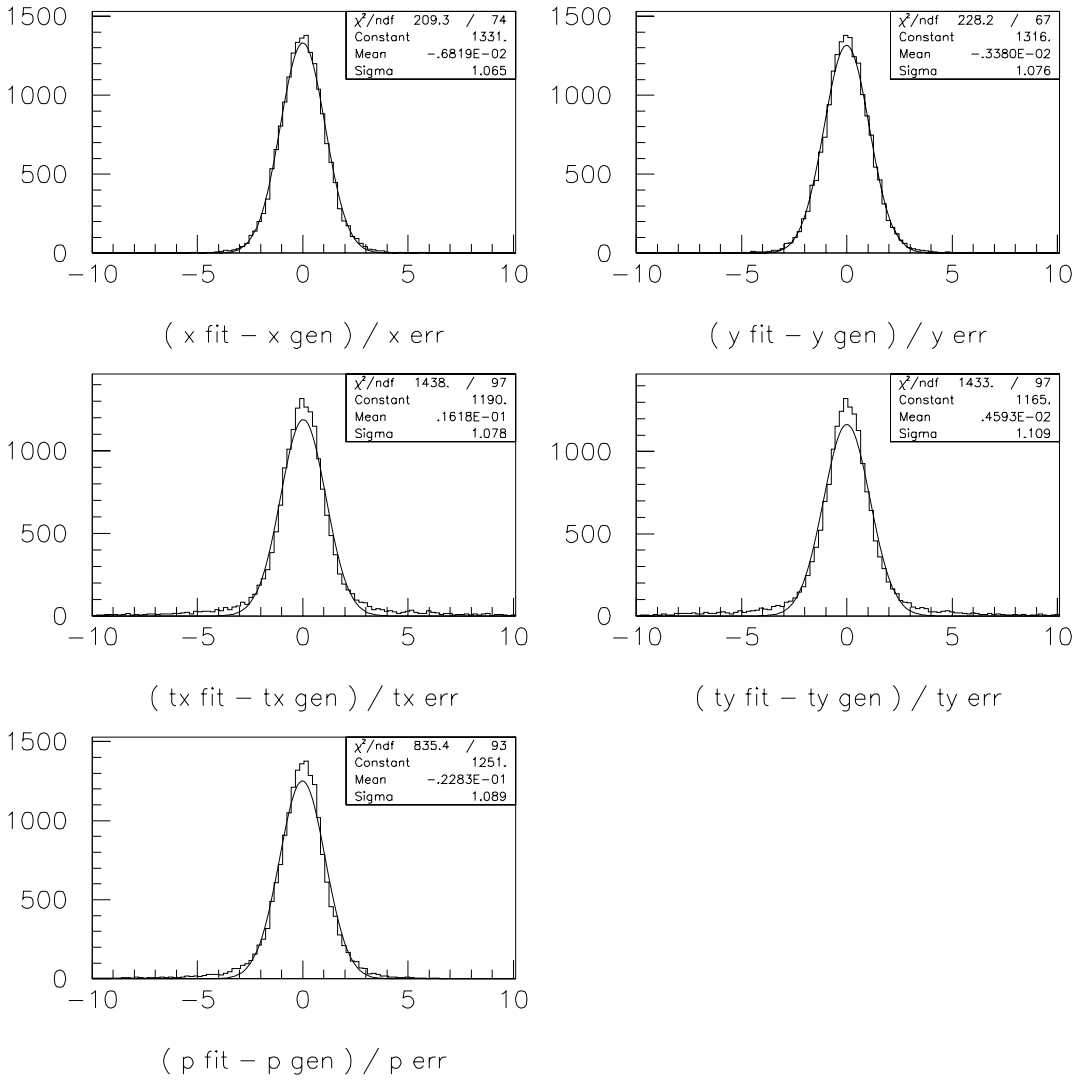

Figure 1: the pull distributions of the fitted track parameters at the track vertex. All distributions are centered on zero and have a sigma close to one.

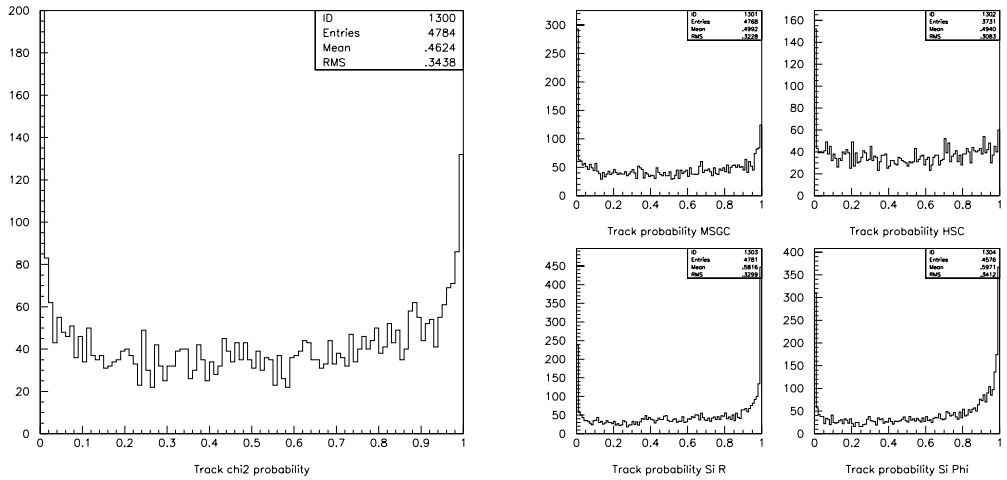

Figure 2: left: the chisquared probability distribution for the overall trackfit; right: chisquared probability distributions for resp. the inner tracker, the outer tracker, silicon r and ϕ parts of the fit.

with small probabilities. The peak at high probabilities ($\sim$ 1) is mainly caused by the vertex detector hits. Here, clusters with only a single strip hit, lead to a non-Gaussian resolution function.

3 Placing The Tracking Stations

The LHCB tracking system has been designed primarily for upstream tracking [2] as described in section 2.1. A number of stations in the field-free region behind the magnet serve to identify track candidates and provide a good "seed" for the track parameters. The remaining stations are used to follow those track candidates "backwards" through the magnet and into the vertex detector. Dividing in this way the tasks of track *finding* and track *following* between separate parts of the tracking system we have chosen the same approach as was used in the design of the HERA-B detector. The comparison with HERA-B has in fact been very useful in designing the LHCB tracking detector.

In the following, we will give an overview of the general considerations that have guided us in the design of the tracking system (section 3.1) as well as of some "hard" boundary conditions that had to be taken into account

[2] A downstream-tracking algorithm is being considered for the 2nd-level trigger. This has been taken into account in the placing of stations upstream of the magnet.

(section 3.2). We will not describe in any detail the different options that were studied, but rather present directly the final layout of the tracking system, in section 3.3. In 3.4, we demonstrate the performance of the system in terms of track following.

3.1 General Considerations

The main tasks taken into consideration in the overall design of the tracking system are pattern recognition (track finding and following) and momentum reconstruction.

No dedicated study has been performed yet on the issue of track finding, i.e. the task of identifying good track candidates in the field-free region behind the magnet. The number of stations reserved for this pupose, as well as their spacing, has been extrapolated from Monte-Carlo studies done by HERA-B [7]. In fact, the setup we have chosen for LHCB closely resembles the HERA-B solution. In LHCB, we have four stations, with a total of 16 (double) detection planes, distributed at equal distances over a total length of 150cm along the beam axis (center of first station to center of last station). HERA-B also has four stations with 16 detection planes, spread out over about 120cm along the beam axis.

Detailed studies have been performed to optimize the positions of the track-following stations. The crucial parameter from the point of view of pattern recognition is the number of candidate hits found per search window when extrapolating a track candidate from one station to the following. This number must be kept small (of order one), as each hit candidate opens a new track candidate that has to be followed. If the number of fake tracks grows too fast, this will impair the performance of the algorithm. The size of the search window is determined by the error on the track extrapolation. It is a function of the knowledge of the track state vector before extrapolation (expressed in its covariance matrix), the amount of material between two stations and the distance over which the track is extrapolated. Track extrapolation is particularly critical on entering the magnetic field, as the limited knowledge of track momentum at this point leads to an additional uncertainty in the particle trajectory. For this reason, it is desirable to place a tracking station in a region, where the magnetic field is still low enough not to disturb the trajectory too much, but already large enough to allow a significantly improved estimate of the track momentum. A reasonable compromise seems to be a point at around 30% of the maximum field strength.

The attainable momentum resolution is mainly determined by the measurement of track parameters in the field-free regions on both sides of the magnet (lever arm). Stations inside the magnetic field do in fact not con-

tribute much to the momentum resolution, they may even diminuish the performance due to the additional multiple scattering and energy loss they introduce. As we will show in section 4.2, momentum resolution in the final setup is in fact dominated by multiple scattering.

The region of highest magnetic field, in the center of the magnet, is considered undesireable also for a different reason: the many curling tracks of low momentum would cause very high occupancies in a tracking station positioned here.

Taking into account that the material introduced by each additional tracking station also increases the occupancy in the following stations by production of secondaries, we can summarize the general strategy as follows:

- a sufficient number of stations in the field-free region behind the magnet, in order to define solid track candidates and provide good seeds for the track parameters
- as few track-following stations as possible, the minimum number being determined by the requirements of pattern recognition
- one station in the downstream "turn-on" region of the magnetic field, to facilitate upstream tracking into the magnet; the same in the region upstream of the magnet, if downstream tracking is required by the trigger algorithms

In addition to these qualitative considerations, which had to be quantified for a variety of scenarios, a number of "hard" boundary conditions had to be taken into account. These will be summarized in the following section.

3.2 Boundary Conditions

Some boundary conditions are imposed on the design of the tracking system by the requirements of, or the interaction with, other detector components:

The RICH detectors require precise predictions of track impact points and track directions for their pattern recognition and momentum analysis. For this reason, both RICH detectors have to be "sandwiched" between tracking stations. These stations, four in total, have to provide good spatial resolution in both horizontal and vertical directions and are equipped with additional detection layers of horizontal wires.

One chamber is needed as close as possible to the exit window of the vertex tank, in order to link tracks into the vertex detector.

The vertex detector itself has been optimized for the reconstruction of primary and secondary vertices. We do not attempt to change the positioning of vertex-detector layers for the purposes of this study.

Station #	z position	main function
1	100 cm	link to vertex detector, RICH 1
2	217 cm	momentum fit, RICH1
3	330 cm	"downstream" tracking
4	425 cm	track following
5	565 cm	track following
6	700 cm	track following
7	790 cm	track finding & momentum seed
8	840 cm	track finding & momentum seed
9	990 cm	track finding & momentum seed
10	940 cm	track finding & momentum seed, RICH2
11	1160 cm	RICH2, link to muon system

Table 2: Positions and main functions of stations in the final setup

It should also be noted that, due to space limitations or interference with other hardware elements in LHCB, not all stations are positioned exactly on the ideal locations as found during the tracking optimisation (e.g. interference of a station frame with the yoke of the magnet).

3.3 The Chosen Setup

As already mentioned in the introduction, we will not attempt to give an account of the different options studied in the optimisation phase, but concentrate on the finally chosen setup. This setup comprises a total of 11 tracking stations, the z positions of which are summarized in table 2. For comparison, figure 3 shows the magnetic field map. The table also summarizes the main functions of each station. Here, we give some more detailed coments:

Stations 1 and 2

Station 1 serves a double purpose. Firstly, it makes the link of the tracking system with the vertex detector. For this, it is placed as close as possible to the vertex tank. But it is also positioned close to the entrance window of the RICH-1 detector and, together with station 2, which is positioned directly behind the RICH, serves to make the necessary precise track predictions for the RICH. Station 2 is also crucial for a precise measurement of the track momentum.

Station 3 and 6

These two stations make the transition from the field-free region to the

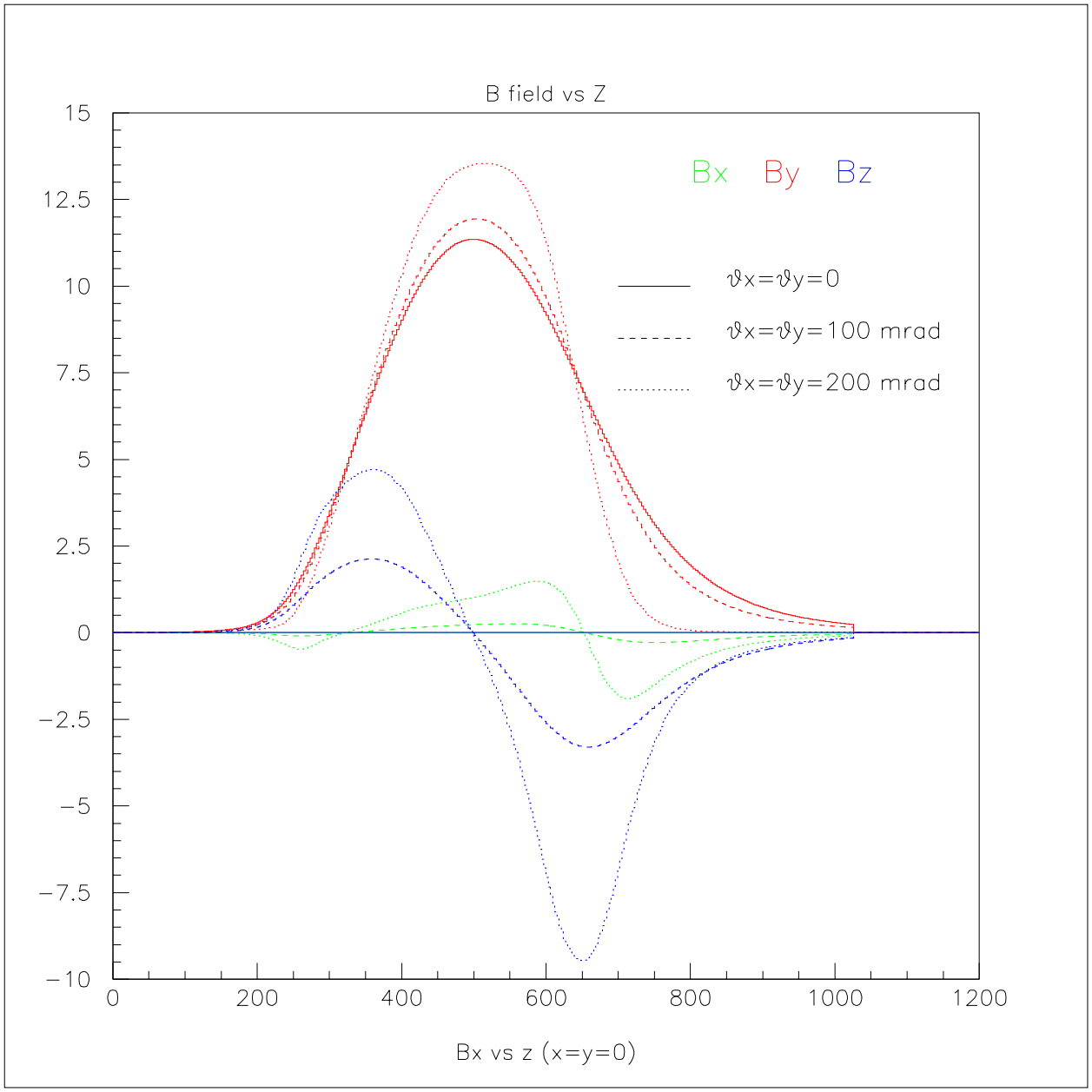

Figure 3: Components of magnetic field as a function of the z position. The different line-types give the field seen by particles under 1) $\vartheta_x = \vartheta_y = 0$, 2) $\vartheta_x = \vartheta_y = 100\,\mathrm{mrad}$, 3) $\vartheta_x = \vartheta_y = 200\,\mathrm{mrad}$

full-field region as discussed in section 3.1. Station 6 fulfills this task for upstream tracking, station 3 for downstream tracking. As station 3 serves no further purpose, it could and should be removed if downstream tracking is not persued in LHCB.

Station 4 and 5

These stations serve to follow tracks through the magnet. They are positioned away from the center of the magnet to avoid the area of highest occupancy.

Stations 7 to 10

These are the track "finding" stations, they serve to provide a good track seed. For this it is important that they have an as large as possible lever arm in a field free region. Station 10, being positioned as close as possible to RICH-2, serves also to provide a track prediction at the entrance to the RICH.

Station 11

Station 11 is positioned directly behind RICH-2 and provides the second track measurement required by the RICH. In addition, it serves to link the calorimeters and the muon chambers with the tracking detector.

3.4 Pattern Recognition in Track Following

In the standard way of track following a track found by the stations in the field free region in the upstream direction is tracked through the magnetic field toward the vertex detector. We have implemented a limited amount of local pattern recognition in this trackfollowing task. At each station we look for candidate tracksegments in a search window which match the track prediction obtained from the downstream chambers.

The typical size of these search windows can be deduced from fig 4, in which we plot the difference of the *predicted* and *true* impact positions of a track. The plot shows that the distribution widens as the track enters the magnetic field (station $6 \rightarrow 5 \rightarrow 4$), narrows when the momentum of the track becomes better measured (station $3 \rightarrow 2$), and finally widens again when the track traverses the RICH1 detector (station $2 \rightarrow 1$).

For downstream tracking, i.e. following the track from a seed in station 1 through the magnet down to station 11, the situation is much worse. No knowledge of the momentum is present up to station 2, leading to root mean square values of several centimeters on entering the magnetic field, as is shown in figure 5. (Note the change of scale for the stations in the magnet.)

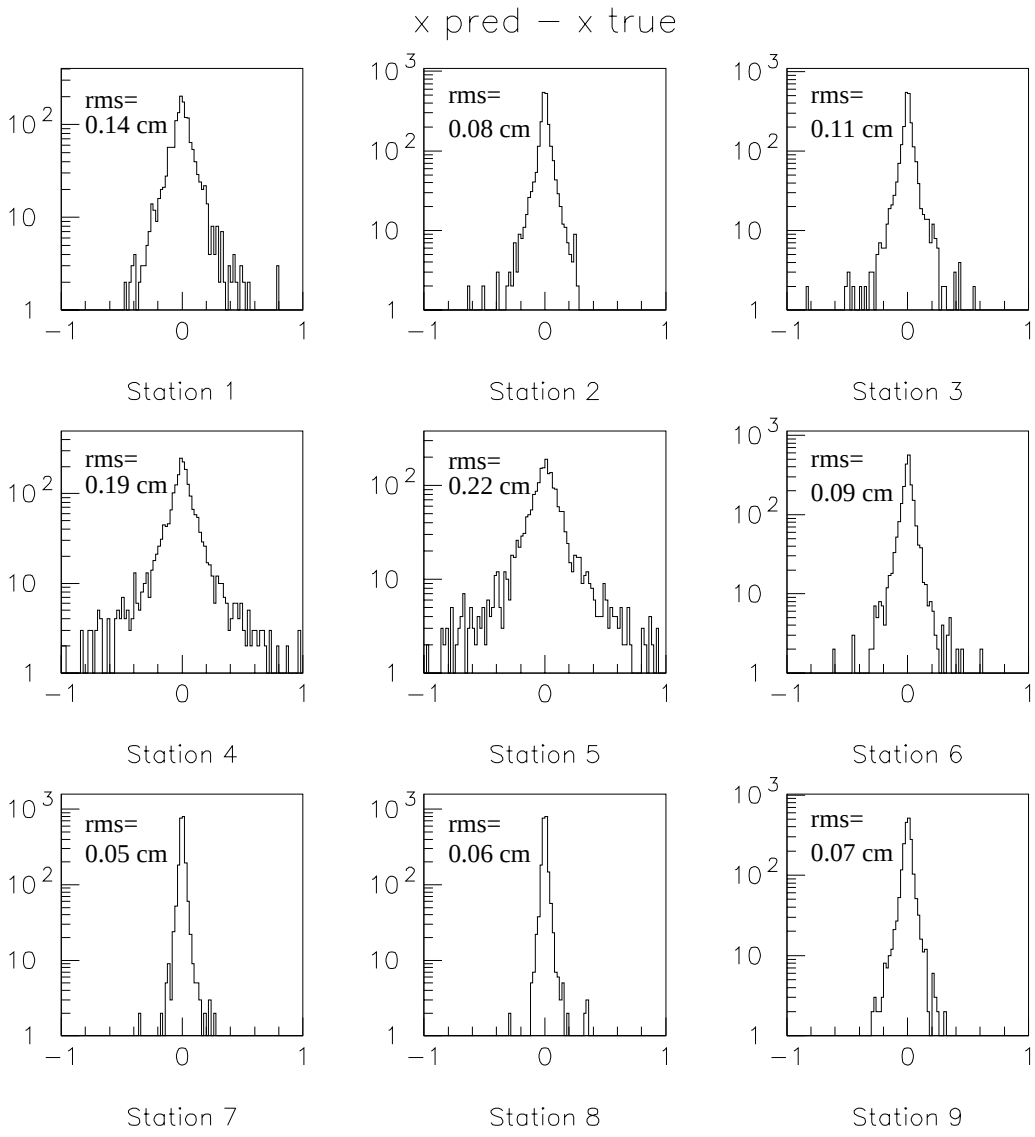

Figure 4: residual distribution $x_{predicted} - x_{true}$ (in cm) for upstream track following

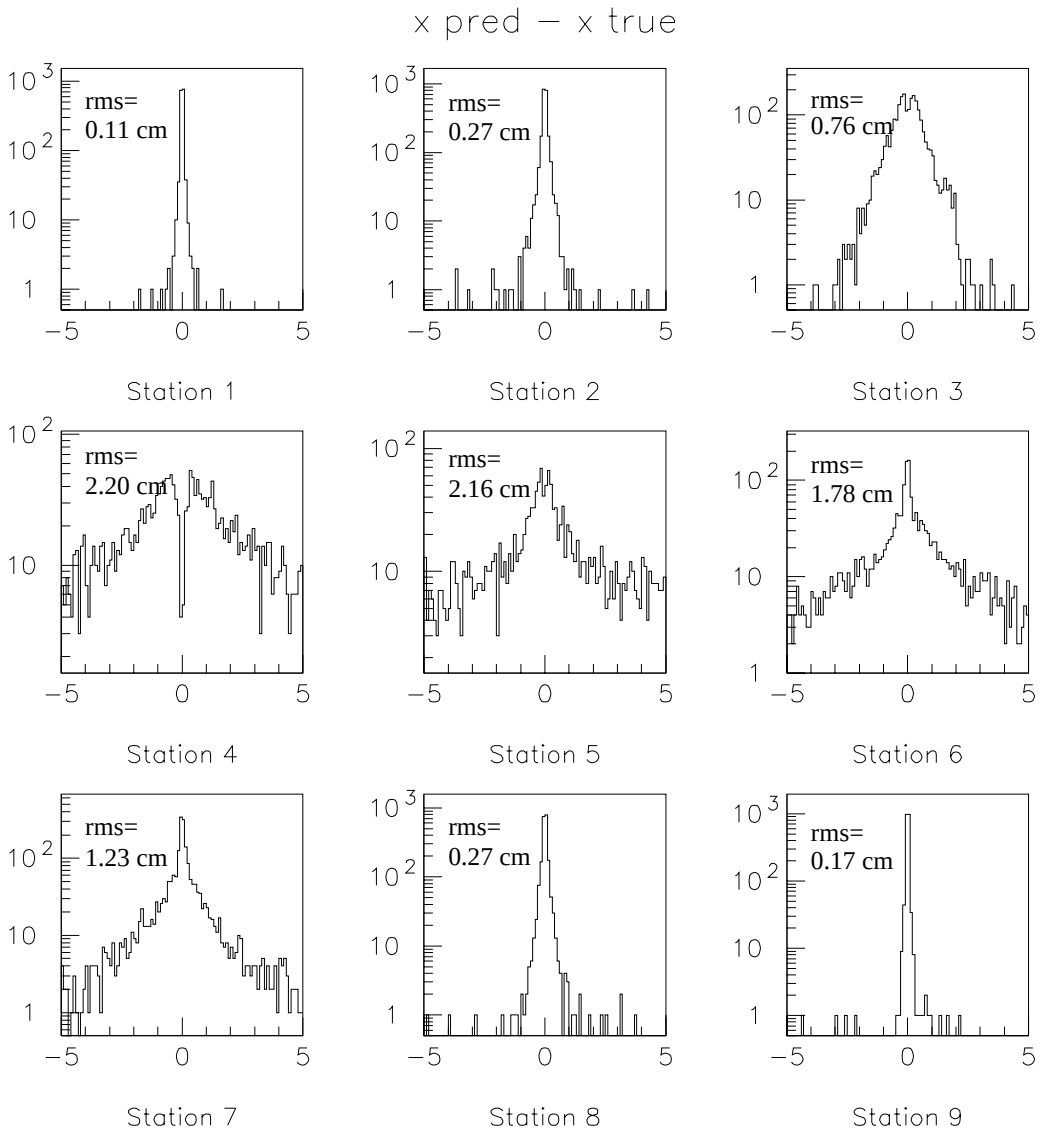

Figure 5: residual distribution $x_{predicted} - x_{true}$ (in cm) for downstream track following

We proceed to form candidate tracksegments by considering all combinations of hits in a search window placed around the track prediction. The size of this searchwindow is conservatively chosen to be 10 standard deviations around the predicted position. A typical size is of the order of 1 to 2 cm, corresponding to only a few channels in the outer tracker but a substantial amount of channels in the inner tracker.

In order to decide whether a track candidate is compatible with the prediction vector (x, y, t_x,t_y,κ) we demand that a quality estimator Q be larger than 0. The quality estimator is defined as [7]:

$$Q = n - w_{\chi^2} \sum_{i=1}^{n} \chi_i^2$$

where the sum runs over all hits in a tracksegment, n, in the station under study, and χ_i^2 is the chisquared contribution of hit i, to the complete track. The weight factor w_{χ^2} is taken to be 0.1. This corresponds to the criterium that on average adding a hit to a track is only done if its χ^2 contribution to the trackfit is less than 10.

The criteria are conservatively chosen in order to cause very small inefficiencies in finding track segments. In the top plots of fig 6 we show the χ^2 contribution of the *worst hit* in a segment which is known to be part of a the track. The acceptance criterium is indicated with a vertical arrow. In the lower plots we show the distribution of the quality Q for these *segments*. Again the vertical arrow shows our acceptance criterium. In summary the inefficiency for dropping the correct track segment with the above criteria is 0.04% for the inner tracker and 0.01% for the outer tracker.

In figure 7 we show, again for upstream track following, the number of track candidates per search window, found by our pattern-recognition algorithm described above.

The stations in the magnet were positioned such that in at most 15% of the cases there is more than just one track-segment candidate.

Finally, in figure 8 we summarize the relative momentum precision $(p_{rec} - p_{gen})/p_{gen}$ at each station during upstream track following.

4 Reconstruction Performance

In this chapter, we demonstrate the overall performance of the proposed tracking system for track reconstruction. In section 4.1, the reconstruction of track parameters is demonstrated, in section 4.2, we discuss contributions to the track momentum resolution, and in section 4.3 examples of invariant-mass resolutions for selected B decay channels are shown.

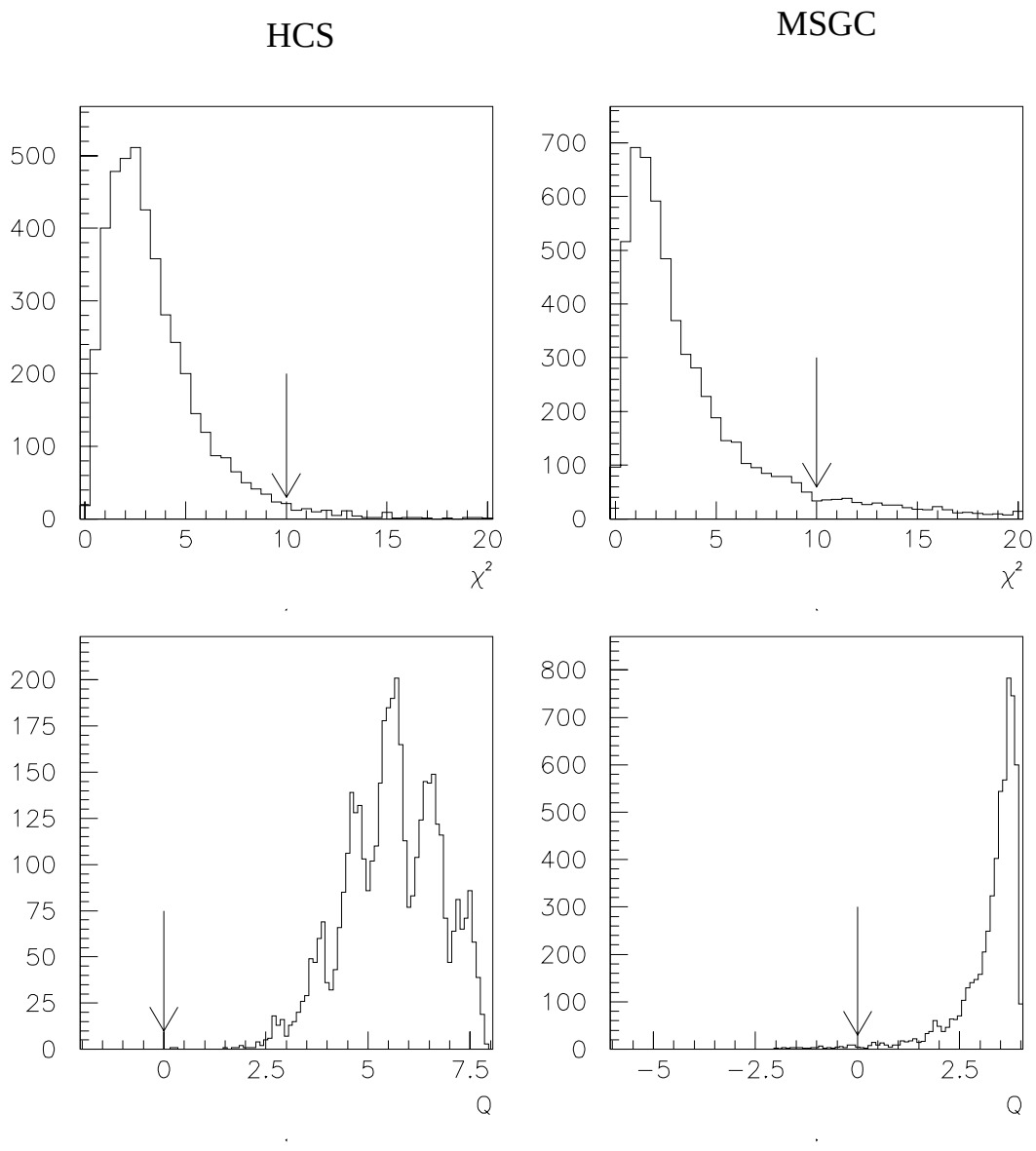

Figure 6: top plots:χ^2 distribution for the worst hit in a track segment inside a station for MC hits that are known to belong to the track. bottom plots: distribution of the quality estimator (see text) for the inner and outer tracker.

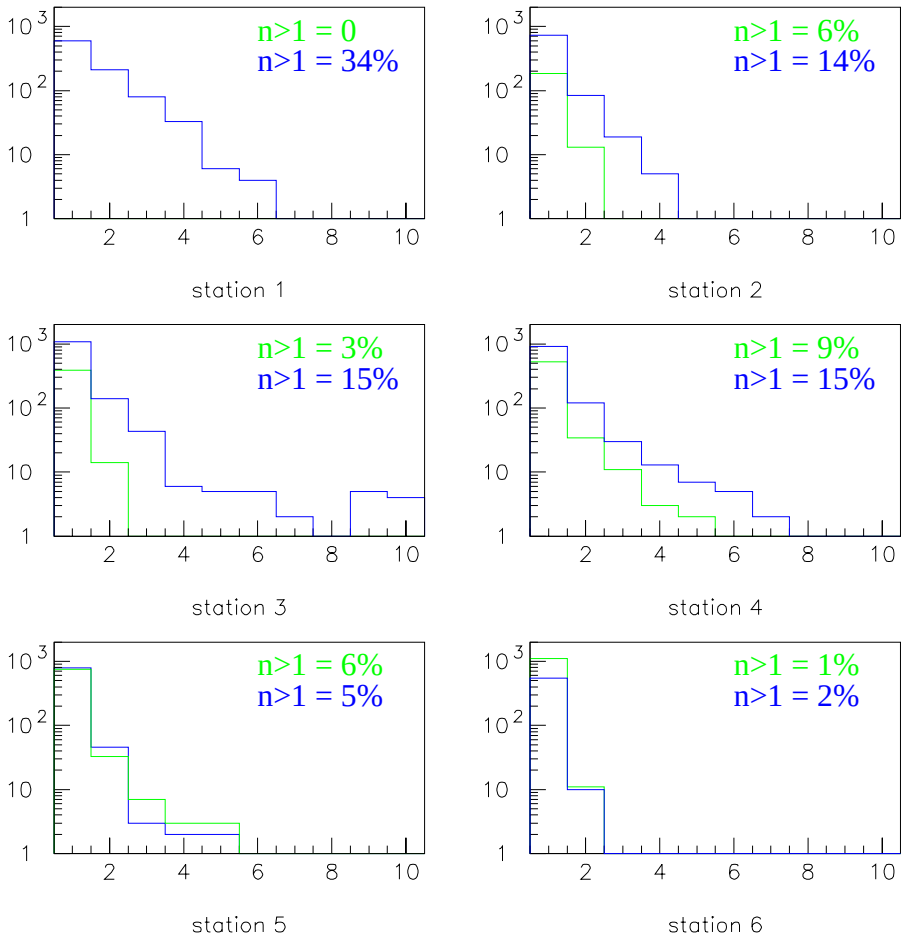

Figure 7: Number of track-segment candidates per search window for upstream tracking. The numbers indicate the percentage of the cases with more than 1 track candidate; in bold print for the inner tracker and in thin print for the outer tracker.

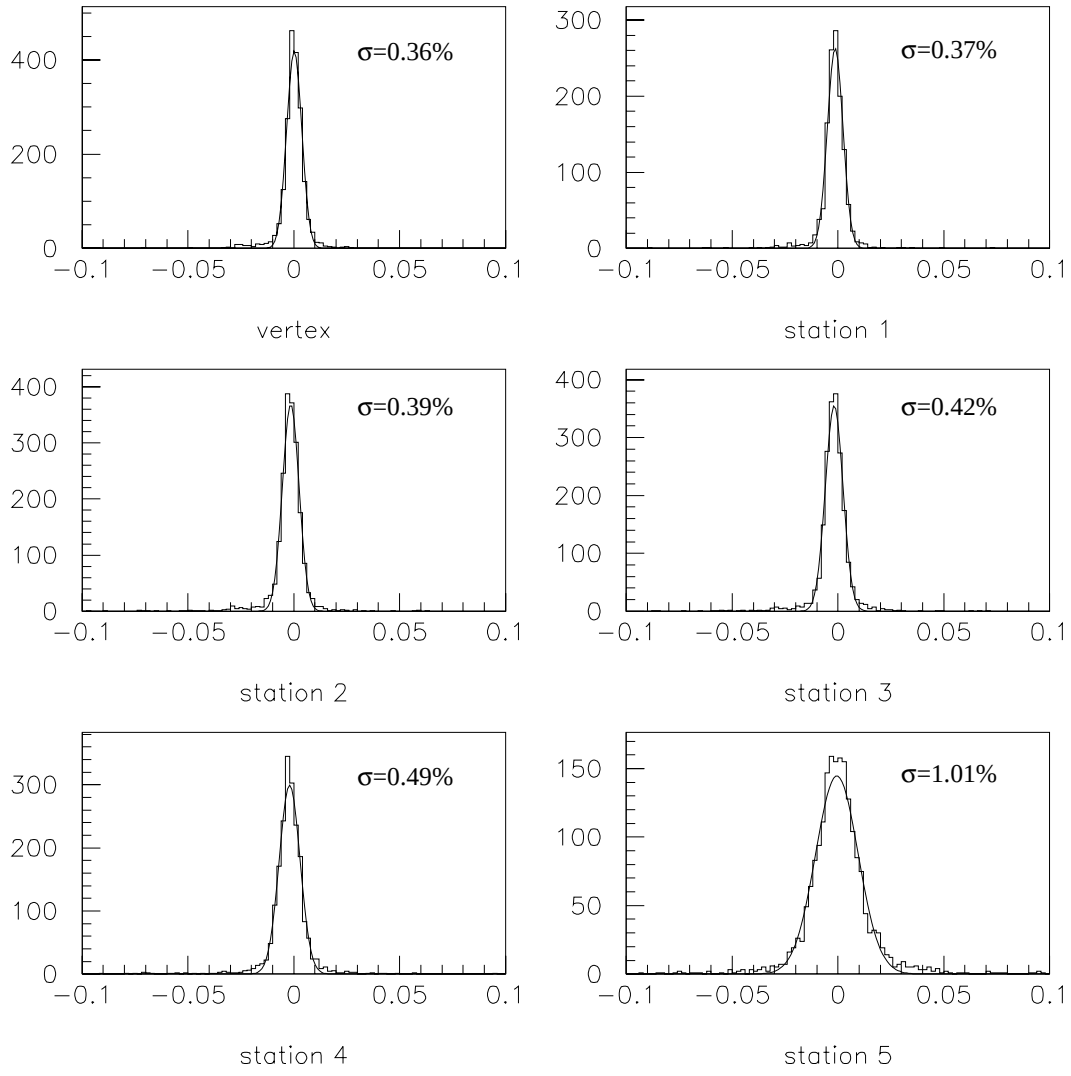

Figure 8: $(p_{rec} - p_{true})/p_{true}$ for **upstream** tracking

4.1 Track-Parameter Resolution

The performance of the tracking system in the reconstruction of track parameters (x,y,t_x,t_y, and momentum) is demonstrated in figure 9. Plotted is the difference between generated and reconstructed track parameters at the z position of the generated origin of the track [3]. The resolutions are around 26 μm x and y coordinates, 3.6×10^{-4} on the slopes and 0.35% on the momentum.

4.2 Momentum Resolution

To first order, we expect the following contributions to the momentum resolution:

- Random change of track direction, due to multiple scattering along the particle trajectory. The average scattering angle is inversely proportional to the momentum, thus $\delta p \,/\, p = C_{ms} \,/\, B$, where C_{ms} is a constant depending on the amount of material traversed.
- Point resolution of the measurements. This contribution is expected to scale as $\delta p \,/\, p = p \cdot C_\sigma \,/\, B$, where C_σ is proportional to the measurement resolution.
- Misalignment of tracking detectors. These introduce a systematic error on the point measurement and lead to correlated errors between the measurements in the different layers in each station.
- Imperfect knowledge of magnetic field map introduces a systematic error that scales as $\delta p \,/\, p = \delta B \,/\, B$.

In the simulation, the systematic effects are neglected, i.e. perfect alignment and perfect knowledge of the magnetic field are assumed. The overall momentum resolution is then of the form:

$$\left(\frac{\delta p}{p}\right)^2 = \left(p \cdot \frac{C_\sigma}{B}\right)^2 + \left(\frac{C_{ms}}{B}\right)^2$$

The momentum resolution as a function of particle momentum is plotted in figure 10. The momentum resolution is, up to 100GeV/c, almost not momentum dependent. From this, we conclude that the multiple scattering contribution is large and that momentum reconstruction is not dominated by the track position measurement. More precisely, fitting the given parametrization to this curve gives $C_{ms}/B = 0.36\%$ and $C_\sigma/B = 0.0024/GeV$.

[3] The reconstructed quantities were obtained extrapolating the track from the first measured point to the vertex z position.

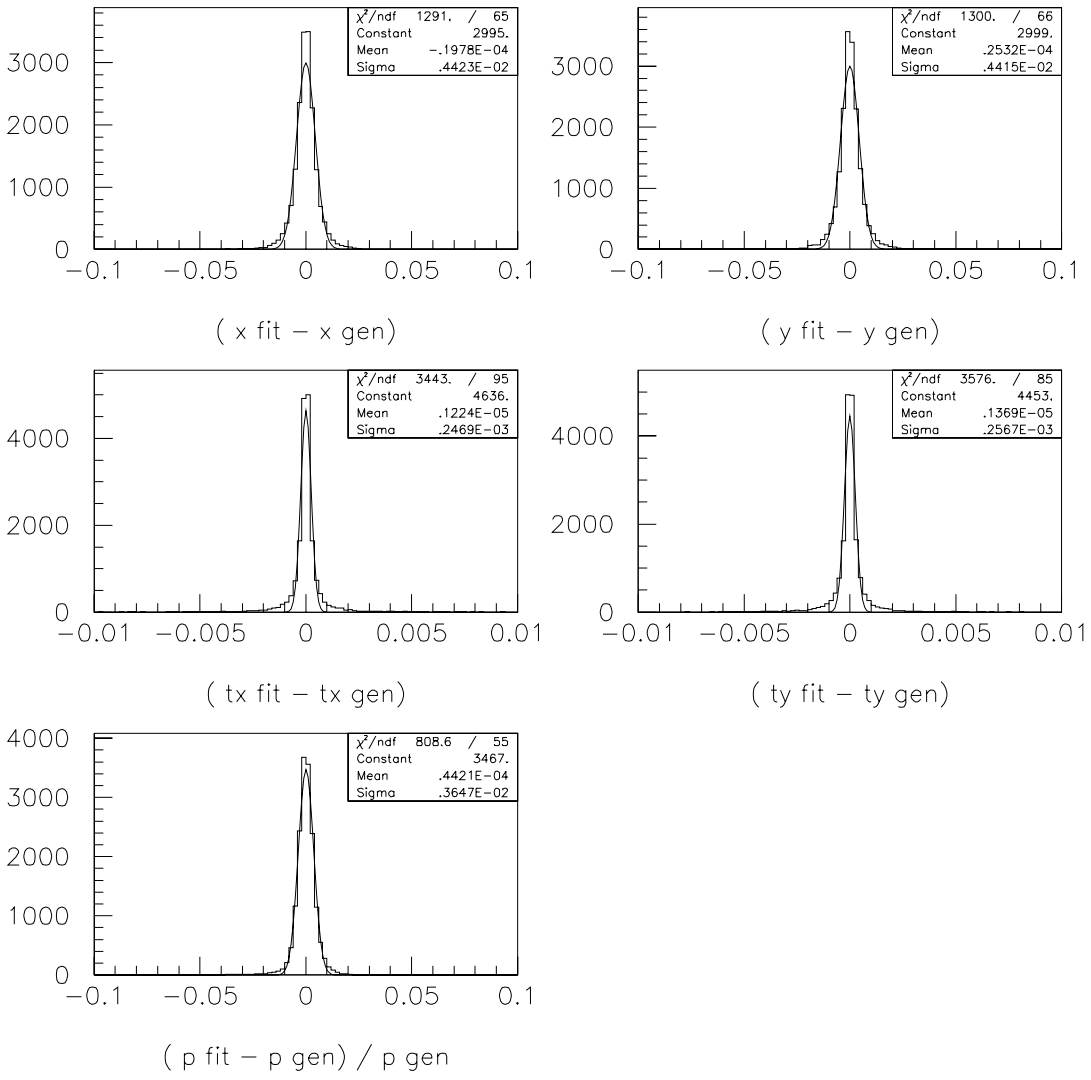

Figure 9: Track parameter resolutions at the generated track origin

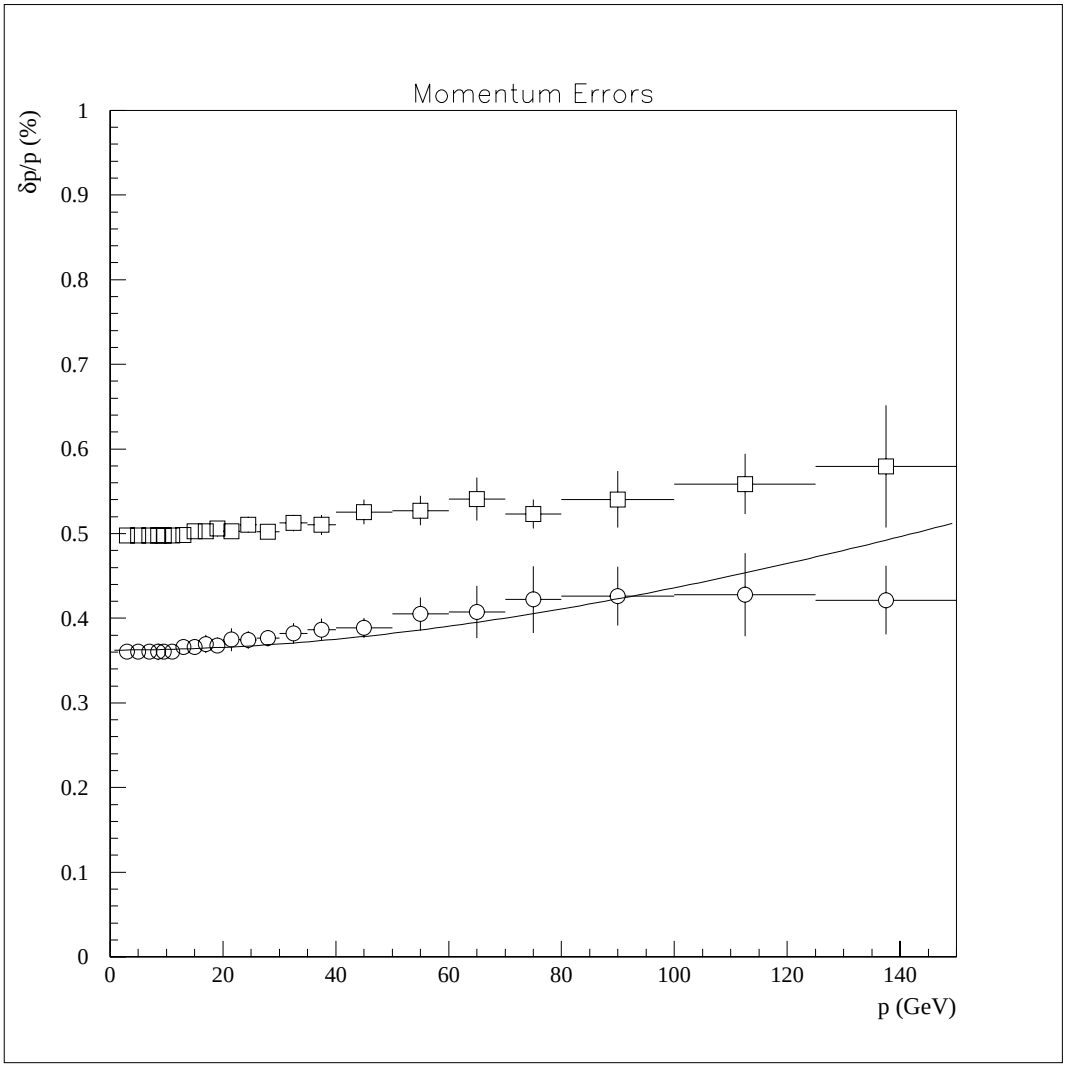

Figure 10: Overall momentum resolution in percentage vs. the particle momentum in GeV. The circles indicate the performance with the nominal setup in LHC-B, the squares indicate the performance in the case all stations would contain twice as much material.

In order to not cause a significant contribution to the resolution, the magnetic field map should be known to better than 0.1 %.

4.3 Invariant-Mass Resolution

The invariant-mass resolution depends on the measurement of the momenta of the decay particles in the tracking system and on the measurements of their slopes in the vertex detector. To estimate the relative weight of the different contributions to the total resolution we have calculated, for two decays with very different topology, the invariant mass using only partially Monte Carlo true information, either momentum or slopes, to find out the contribution of the reconstructed slope or momentum respectively.

Figure 11 shows the difference between the recontructed and the true masses for the two decays studied: $B^0 \to \pi^+\pi^-$ and $D_s \to \pi K^+ K^-$ for D_s's from $B_s \to D_s\pi$. In both cases, the daughter particles are identified using Monte Carlo information. Two hits in the silicon vertex detector were required in every track and a cut on the quality of the momentum measurement was applied: if the difference between reconstructed and generated momentum in any of the decay products is larger than three times its error, the event was not used. The mass resolutions are 4.2 MeV and 15.2 MeV for the D_s and the B^0 respectively.

The different contributions to the mass resolution can be studied by replacing the reconstructed slopes and/or momenta by the generated ones. The result of this study is shown in figure 12 for the D_s case. The sigma of a gaussian fit to the distribution is 2.9 MeV when the Monte-Carlo slopes are used and 2.6 MeV when the momenta are taken from the Monte Carlo. For the B^0, figure 13, the same fits give 14.4 MeV and 4.2 MeV. These numbers have to be compared with the resolution of 4.6 MeV and 15.2 MeV we have when we use only reconstructed information. Our conclusions are that in the $B^0 \to \pi^+\pi^-$ the mass resolution is effectively determined by the momentum measurement in the spectrometer, while in the $D_s \to \pi K^+ K^-$ decay the measurement of the momenta and slopes of the tracks contribute equally.

The bottom plots in figures 12 and 13 show $r(\theta)$ and ϕ measurement contributions to the total mass resolution.

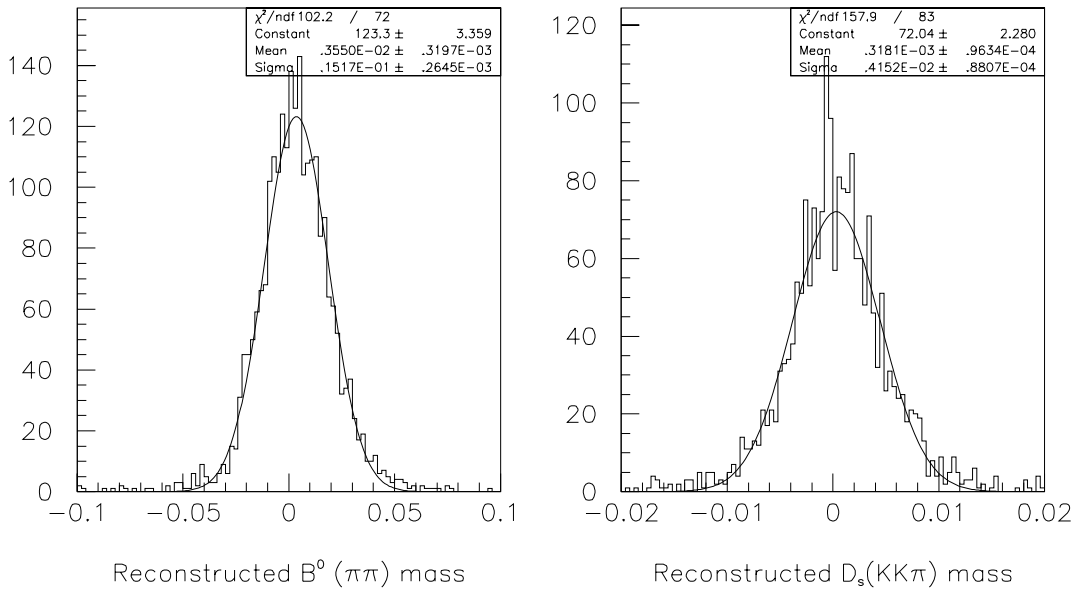

Figure 11: Reconstructed - true masses for D_s and B^0.

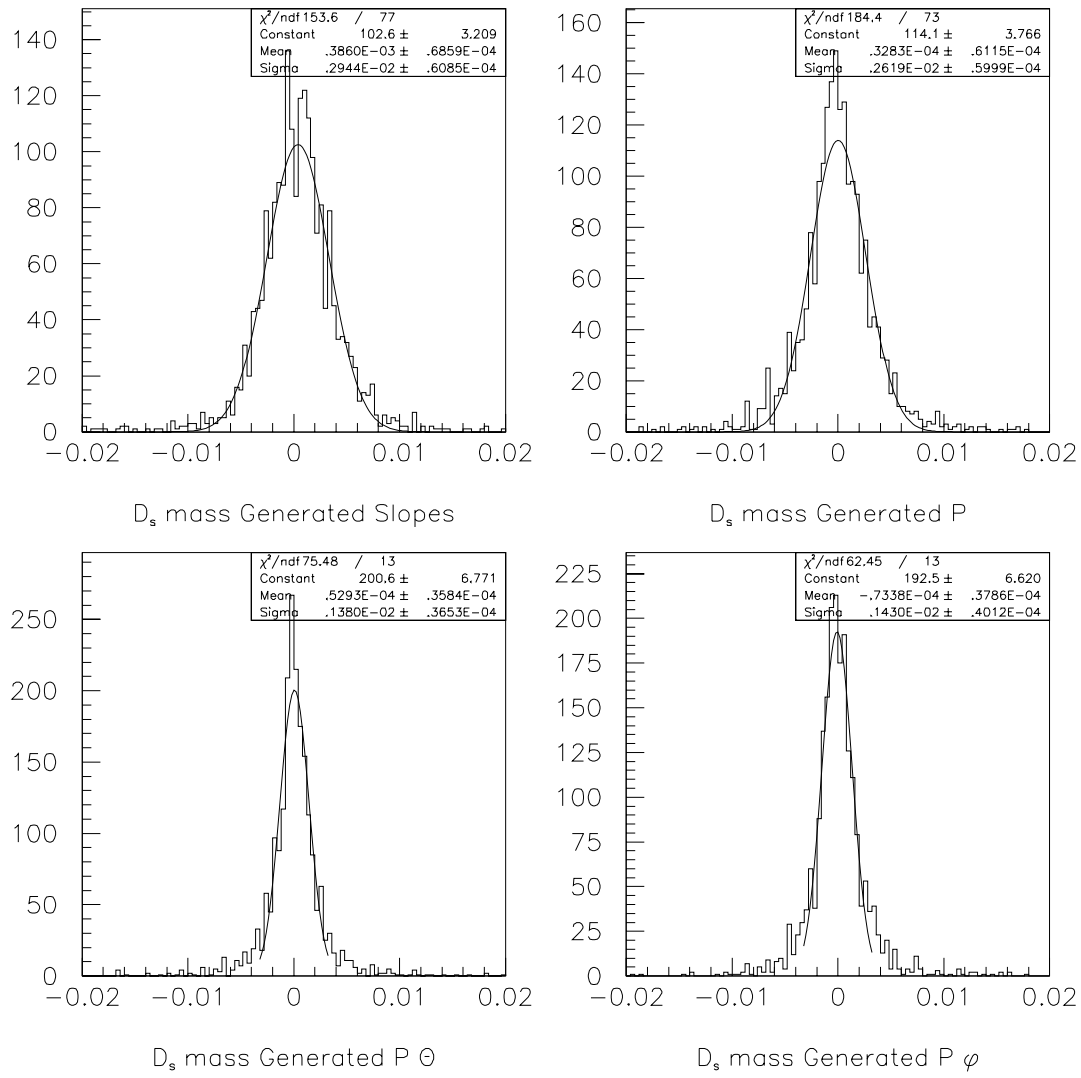

Figure 12: Breakdown of contribution of mass resolutions of the D_s. *upper-left:* Contribution of measured track momenta, *upper-right:* Contribution of measured track slopes, *lower-left:* Contribution of measured phi angles, *lower-right:* Contribution of measured theta angles

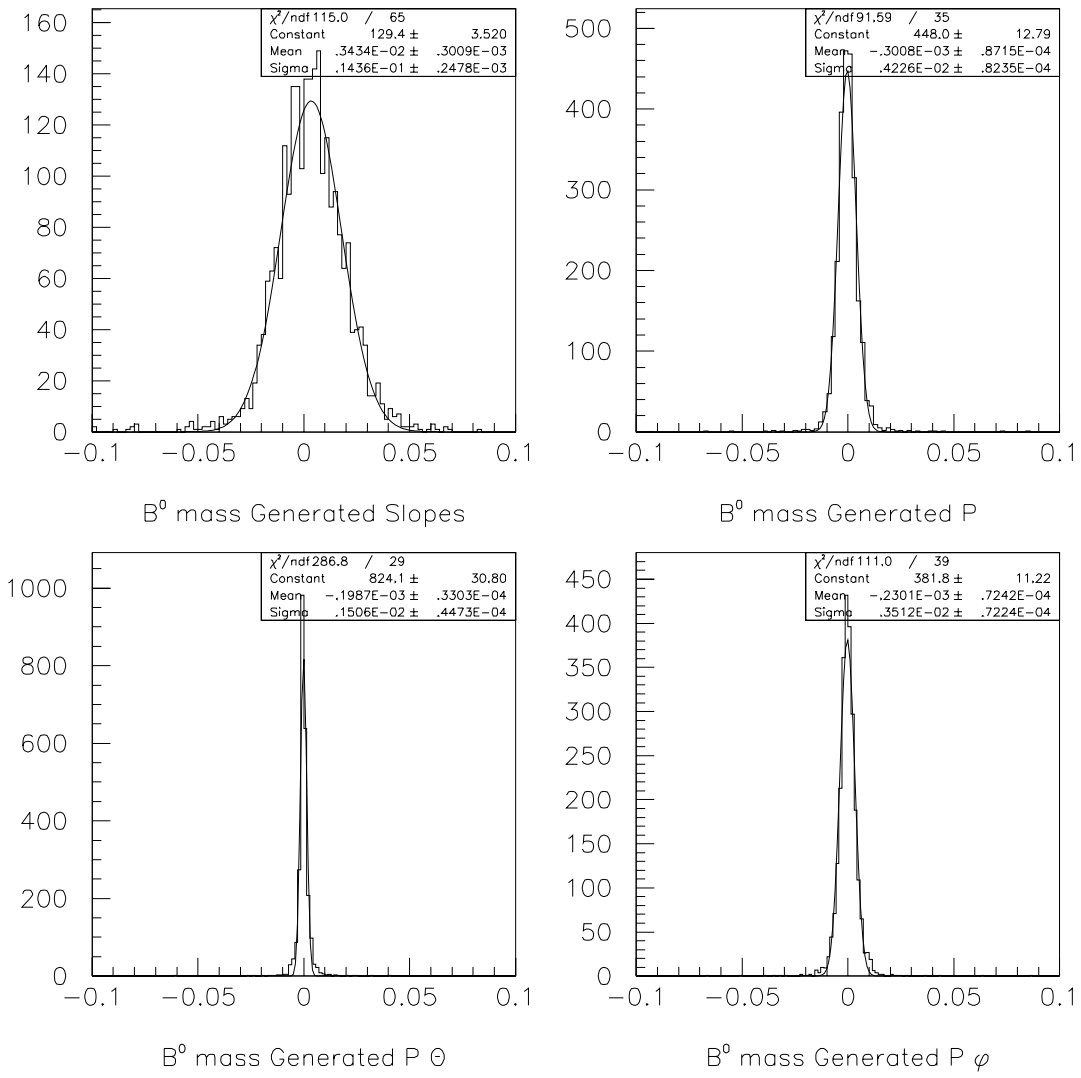

Figure 13: Breakdown of contribution of mass resolutions of the B^0. *upper-left:* Contribution of measured track momenta, *upper-right:* Contribution of measured track slopes, *lower-left:* Contribution of measured phi angles, *lower-right:* Contribution of measured theta angles

Acknowledgements

In the implementation of a Kalman Filter based trackfit for LHCB we have greatly benefitted from the work done for the HERA-B experiment. In particular we would like to thank Thomas Lohse and Rainer Mankel for sharing their experience and for stimulating discussions.

References

[1] M. Merk, "Digitizations and Occupancies for Tracking in LHC-B", LHC-B note.

[2] A. Tsaregorodtsev, "SICB user guide, GEANT3 based simulation package for the LHC-B Experiment", june 19, 1997

[3] R. Mankel, "Application of the Kalman Filter Technique in the HERA-B Track reconstruction", HERA-B note 95-239.

[4] H.A.Bethe, Phys. Rev. 89 (1953) 1256

[5] D. Stampfer, M. Regler, R. Frühwirth,"Track fitting with energy loss", Com.Phys.Commun. 79 (1994) 157-164

[6] H.A.Bethe and W.Heitler, Proc. Roy. Soc. A146 (1934) 83.

[7] R. Mankel, "*ranger* a Pattern Recognition Algorithm for the HERA-B Main Tracking System", HERA-B note 97-082.